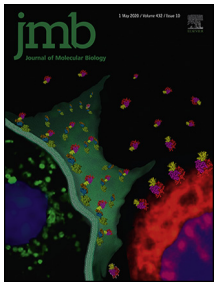

Pulmonary Surfactant Lipid Reorganization Induced by the Adsorption of the Oligomeric Surfactant Protein B Complex

Juho Liekkinen [1,2], Giray Enkavi [1], Matti Javanainen [1,2,3], Barbara Olmeda [4,5], Jesús Pérez-Gil [4,5] and Ilpo Vattulainen [1,2,6 †]

*1 - **Department of Physics,** University of Helsinki, Helsinki, Finland*
*2 - **Computational Physics Laboratory,** Tampere University, Tampere, Finland*
*3 - **Institute of Organic Chemistry and Biochemistry,** Czech Academy of Sciences, Prague 6, Czech Republic*
*4 - **Department of Biochemistry,** Faculty of Biology, Complutense University of Madrid, Madrid, Spain*
*5 - **"Hospital 12 Octubre (imas12)" Research Institute,** Madrid, Spain*
*6 - **MEMPHYS—Centre for Biomembrane Physics***

***Correspondence to Jesús Pérez-Gil and Ilpo Vattulainen:**. jperezgil@bio.ucm.es, ilpo.vattulainen@helsinki.fi*
https://doi.org/10.1016/j.jmb.2020.02.028

Abstract

Surfactant protein B (SP-B) is essential in transferring surface-active phospholipids from membrane-based surfactant complexes into the alveolar air–liquid interface. This allows maintaining the mechanical stability of the surfactant film under high pressure at the end of expiration; therefore, SP-B is crucial in lung function. Despite its necessity, the structure and the mechanism of lipid transfer by SP-B have remained poorly characterized. Earlier, we proposed higher-order oligomerization of SP-B into ring-like supramolecular assemblies. In the present work, we used coarse-grained molecular dynamics simulations to elucidate how the ring-like oligomeric structure of SP-B determines its membrane binding and lipid transfer. In particular, we explored how SP-B interacts with specific surfactant lipids, and how consequently SP-B reorganizes its lipid environment to modulate the pulmonary surfactant structure and function. Based on these studies, there are specific lipid–protein interactions leading to perturbation and reorganization of pulmonary surfactant layers. Especially, we found compelling evidence that anionic phospholipids and cholesterol are needed or even crucial in the membrane binding and lipid transfer function of SP-B. Also, on the basis of the simulations, larger oligomers of SP-B catalyze lipid transfer between adjacent surfactant layers. Better understanding of the molecular mechanism of SP-B will help in the design of therapeutic SP-B-based preparations and novel treatments for fatal respiratory complications, such as the acute respiratory distress syndrome.

Introduction

Pulmonary surfactant (PSurf) is an essential lipid–protein complex that covers the alveolar epithelium and maintains the gas-exchange interface at the respiratory surface. The main biophysical function of PSurf is to decrease the surface tension at the air–water interface, thus reducing the work needed for breathing and preventing alveolar collapse at exhalation [1]. The PSurf consists of approximately 80% of zwitterionic phospholipids, 10% of neutral lipids [mostly cholesterol (CHOL)], and 8%–10% of hydrophobic and hydrophilic surfactant proteins (SPs) [1–3]. While the hydrophilic SPs (SP-A and SP-D) are mainly involved in the innate immune mechanisms in the alveoli [4–6], the hydrophobic SPs (SP-B and SP-C) together with the surfactant lipids play crucial roles directly in the biophysical function of the PSurf [7]. The three most important biophysical properties of functional PSurf films are rapid adsorption to the air–water interface, efficient compression during exhalation, and efficient re-extension upon expansion during inhalation [1,4,8]. These qualities of the PSurf depend on the highly optimized interplay

between different lipid species and the hydrophobic SPs [4,7].

Saturated zwitterionic dipalmitoylphosphatidylcholine (DPPC) is the most abundant phospholipid in the PSurf (~40% by total mass) and is responsible for the efficient surface tension reduction property of the surfactant [7,9,10]. Unsaturated zwitterionic phosphatidylcholine and unsaturated anionic phospholipids, mostly phosphatidylglycerol (PG), make up a majority of the rest of the phospholipid fraction [1]. The composition of the PSurf is highly regulated and optimized as to the proportions of surface-tension-lowering (saturated) and fluidizing (unsaturated) lipid components [11,12]. Neither lipid type can alone support both the surface active and the fluidic nature of the PSurf at physiological temperatures [13]. Moreover, specific protein–lipid interactions between the lipids and SPs are required for efficient surfactant film formation and re-extension at the air–water interface [4,13,14].

One of the key proteins of the PSurf is the pulmonary SP-B (see Figure 1). This protein partitions to the disordered lipid phases while binding to the surface of PSurf bilayers and monolayers with a preference for interacting with anionic phospholipids, like PG [15–18]. It participates in the packaging and exocytosis of the PSurf in the form of tightly packed lamellar bodies from the ATII cells into the aqueous phase [19]. SP-B also catalyzes efficient transfer of lipids between membranes and surfactant monolayers. This way, it enhances packing and re-extension of the surface-active lipid species during the compression–expansion cycles of breathing, promoting the formation, adsorption, and stabilization of the PSurf film at the air–water interface [9,12–14,20–23]. As an essential component of the PSurf complex, the complete lack of SP-B results in a lethal respiratory failure at birth [24,25]. Partial deficiency or inactivation of SP-B has been also associated with severe respiratory pathologies such as acute respiratory distress syndrome [26–28]. Development of a functional, safe, and affordable synthetic alternative for the current animal-derived surfactants used in surfactant replacement therapy [29] in the treatment of preterm neonates and acute respiratory distress syndrome patients depends on our understanding of the underlying mechanism of the function of SP-B and its derivatives.

SP-B belongs to the saposin-like protein (SAPLIP) family, which consists of lipid-interacting proteins with diverse functions sharing a common fold [30]. SP-B is a highly hydrophobic, 79-residue polypeptide chain with a molecular mass of 8.7 kDa and a net positive charge of 7 [31,32]. Like other SAPLIP members, SP-B contains three intra-chain disulfide bridges that stabilize its fold. In the airways, SP-B appears in dimeric form [33], in which the monomers are connected by an inter-chain disulfide bridge at C48 [32,34]. The dimerization of SP-B is involved in its surface tension reduction function [33]. Although the atomistic structure and the molecular mechanism of SP-B remain elusive [31,35], our recent studies [19,35] have revealed higher-order SP-B oligomers consisting of several SP-B dimers.

To account for the higher-order oligomerization of SP-B, we previously proposed a new structural model for SP-B: a supradimeric oligomer model with *n*-fold circular symmetry [19,35]. In this model, dimeric units of SP-B homology modeled based on the dimeric saposin B [Protein Data Bank (PDB) ID: 1N69, Figure 1(a)] [36], another member of the SAPLIP family, are arranged in a ring shape allowing formation of the characteristic intra-chain disulfide bridge at C48 between the neighboring monomers. Such an SP-B dimer [Figure 1(b)] modeled based on saposin B structure accommodates all three intra-chain disulfide bridges (C8–C77, C11–C71, and C35–C46) [34], but not the inter-chain disulfide bridge (C48) [34] characteristic to SP-B [Figure 1(c) and (d)]. A ring-like multidimeric model, however, can conceivably contain the inter-chain disulfide bridge between the neighboring dimers. In addition, each dimer in such multidimeric model can enclose a phospholipid molecule between the monomers forming a putative lipid-binding pocket [Figure 1(b)], similar to the one in the closed saposin B conformation [36]. Moreover, the hydrophobic lining of the central pore in the middle of the oligomer ring [Figure 1(g)] suggests a potential mechanism for lipid transport through this channel [35].

The discovery of functional higher-order oligomers has led to various hypotheses on the molecular mechanism of SP-B and the role of other surfactant components in its oligomerization. Olmeda *et al.* suggested that two SP-B oligomer rings can bridge nearby PSurf membranes by forming a hydrophobic tube, which would facilitate rapid flow of surfactant lipids between the membranes through the hydrophobic central pore of the oligomers [35]. In this way, SP-B is thought to function as a key protein to promote lipid transfer between the surfactant storage structures and the monolayer film, which covers the air–liquid interface at the surface of the alveoli [14]. The oligomerization state of SP-B is driven by the molecular composition of the lipid environment, and by the presence and amount of SP-C [28,35,37]. SP-B establishes selective interactions with anionic lipids [17,18]. Specifically, PG has been suggested to facilitate the oligomerization of SP-B in membranes [35,37], which enhances SP-B activity. Moreover, the lipid transfer activity of SP-B is disrupted by large amounts of CHOL [38,39], but this effect is counteracted with the inclusion of SP-C. Meanwhile, SP-C has been shown to dissociate and modulate the oligomerization of SP-B by forming SP-B/SP-C complexes [37].

In this study, we investigated the functional and structural implications of supra-dimeric ring-like oligomers of SP-B and its structural units, namely, the

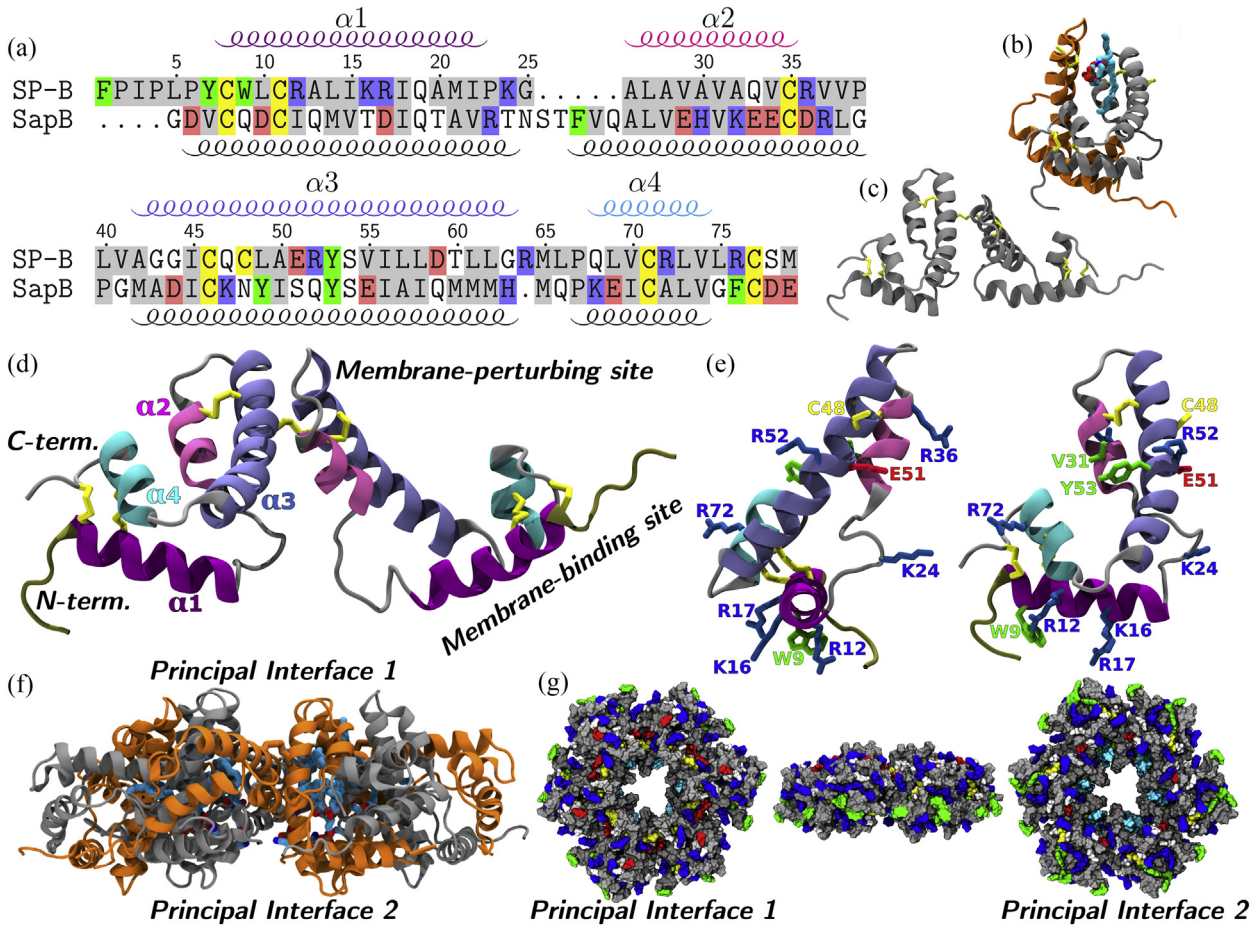

Figure 1. The structures of SP-B used in this study are based on a homology model with saposin B. (a) Sequence alignment of SP-B and saposin B shows the identities of the most important residues in the SAPLIP fold. The alpha-helical segments are shown as spirals. (b) The functional dimer consists of two non-covalently bound SP-B monomers modeled based on the crystal structure of saposin B (PDB ID: 1N69). A POPE lipid docked into the putative lipid-binding cavity is shown in liquorice (cyan). (c, d) The disulfide-bridged dimer is covalently attached at C48 (yellow). The N-terminal insertion sequence (N-term., SP-B_{1-7}, brown), helix 1 (α1, SP-B_{8-22}, purple), helix 2 (α2, SP-B_{26-35}, pink), helix 3 (α3, SP-B_{42-63}, light blue), and helix 4 (α4, SP-B_{68-74}, cyan) are shown in the structure. The residues at the turn of the secondary structure (SP-B_{36-45}) form the membrane-perturbing site, while the membrane-binding site consists of the N-terminal insertion sequence, helix 1, and the C-terminal helix 4. (e) Positions of the specific residues discussed further in the text. (f) The SP-B hexamer has two main membrane-interacting interfaces: Principal Interface 1 has the membrane-perturbing sites rotated toward its respective membrane, while Principal Interface 2 has the membrane-binding sites including the N and C termini of the dimeric subunits toward the membrane. (g) Hydrophobic residues (gray), positively (blue) and negatively (red) charged residues, aromatic residues (green), neutral residues (white), and cysteines (yellow) shown at the surface of the SP-B hexamer structure.

"functional dimer" [Figure 1(b)] and the "disulfide-bridged dimer" [Figure 1(c)]. We refer to the dimer formed by two SP-B monomers in a conformation akin to that of saposin-B and without the inter-chain disulfide bridge at C48, the functional dimer. Because the structure of the functional dimer is based on the saposin B structure, the hydrophobic interface between the monomers contains a putative lipid-binding pocket, and it can be in either an open or closed conformation based on the relative position of the monomers. We chose to concentrate on the closed conformation that already encloses a phospholipid in the saposin B model [36]. The disulfide-bridged dimer, on the other hand, refers to the two neighboring chains in the supra-dimeric model that form a dimer-stabilizing interface containing C48, E51, and R52 [Figure 1(e)]. These dimers are covalently bonded at C48 and form the structural subunit of the supra-dimeric model. We note that the exact number of dimers in the multidimeric complex is not known [35,37]. Originally, particles of SP-B consistent with this supramolecular organization were isolated from detergent-solubilized surfactant preparations and imaged by electron microscopy (EM) and atomic

force microscopy [35], and SP-B was suggested to organize into oligomers of diverse sizes [35]. We therefore initially generated supradimeric models with circular symmetry of a range of number dimers for this study. However, we focused on the hexameric models in our simulations for feasibility. The hexamers fit well into the EM density [35], being currently the best structural model for SP-B.

We used extensive coarse-grained (CG) molecular dynamics (MD) simulations to explore the biophysical properties of SP-B that emerge from its higher-order oligomerization [19,35], and to clarify how these properties are involved in the various biological functions of SP-B. Particular attention was paid to the protein–lipid interactions associated with the different oligomeric states of SP-B to clarify their role in the oligomerization and membrane binding of the protein complex. Since these research themes focus on molecular processes that take place on short time scales, computer simulations are here the method of choice. Previous studies have shown that biomolecular simulations can reveal new exciting phenomena and, besides, help to interpret existing experimental observations [40,41]. In the context of PSurf, previous biomolecular simulations have been successful in, for example, describing the folding of lipid layers at the water–air interface during compressions and expansionsexpansions, and in explaining how SP-B monomers and dimers mediate lipid flow between monolayers and bilayers [42–45].

Our results suggest two important lipid interaction sites in the structure of the SP-B hexamer. First, the N- and C-terminal hydrophobic and positively charged residues are essential for the formation of a functional membrane-binding mode. Meanwhile, the hydrophobic central pore of the SP-B ring is involved in the lipid transfer activity of SP-B. The SP-B hexamer features membrane-perturbing active sites, which cause lipid protrusion into the central pore of the SP-B ring. The resulting lipid neck suggests a new molecular mechanism for lipid transfer by SP-B. Finally, the results provide an explanation as to how the lipid composition of the PSurf affects the membrane binding and the activity of SP-B: in essence, PG and CHOL have a cooperative effect, where PG interacts with the positively charged residues in the protein, and CHOL binds to specific high-affinity binding sites found in the structure of the SP-B hexamer.

Results

Membrane-binding mode and lipid–protein interactions of the dimeric SP-B units

We first investigated the lipid–protein interactions in the functional [Figure 1(b)] and disulfide-bridged dimer [Figure 1(c)] using lipid self-assembly simulations. In these simulations, the positions of the lipid molecules were initiated randomly, and they were allowed to assemble into membranous structures. The use of the standard MARTINI model [46–49] allows for a high-throughput simulation method to perform unbiased protein–membrane-binding studies. These simulations helped us characterize possible membrane-binding modes of the dimer units and define important lipid–protein binding sites in the SP-B structure. We took advantage of this information in designing the membrane-binding simulations of the SP-B hexamer. A detailed description of the binding modes of the dimers is discussed in the Supporting Information (SI) (see Section S2.1). Here, we only provide a brief description highlighting the most essential features.

Our simulations revealed that the functional dimer [Figure 1(b)] binds the membrane in two different peripheral (surface-bound) modes (Figures S1, S2, and S3), whereas the disulfide-bridged dimer [Figure 1(c)] can be found embedded more deeply into the membrane (Figures S4 and S5). In the first mode of the functional dimer, the hydrophobic and positively charged residues in the N-terminal insertion sequence ($SP\text{-}B_{1–7}$), the amphiphilic helix 1 ($SP\text{-}B_{8–22}$), and the C terminus ($SP\text{-}B_{63–79}$) interact with the head group region of the membrane. For simplicity, we named the interface of the functional dimer that interacts with the above-mentioned regions the *membrane-binding site* [Figure 1(a)]. In this mode, W9 and the three positively charged residues on helix 1 (R12, K16, and R17) [see Figure 1(e)] interact specifically with the membrane, especially with palmitoyloleoylphosphatidylglycerol (POPG; Figure S3). In the second mode, the positively charged and hydrophobic residues in the bend between helices 2 and 3 ($SP\text{-}B_{36–45}$) are involved in membrane binding. In this mode, the opening of the lipid-binding cavity faces the membrane and the binding causes perturbation of the nearby lipid head groups and acyl chains (Figure S1). Thus, we named this interface of the functional dimer the *membrane-perturbing site* [Figure 1(a)]. Furthermore, our simulations showed that the disulfide-bridged dimers can oligomerize on bilayers (Figure S6), which causes large lipid protrusions.

Membrane-binding modes of the SP-B hexamer

To get an unbiased view of the possible lipid-binding modes of the SP-B hexamer, we considered four different lipid compositions (Table S1) in lipid self-assembly simulations. These simulations result in a multitude of lipid structures. We focus here only on a subset of self-assembly simulations, which resulted in the formation of continuous bilayers as successful self-assembly attempts. In these simulations, SP-B hexamer binds the bilayers peripherally with lipids filling its central cavity, regardless of the lipid composition used.

The SP-B hexamer binds the bilayers in two distinct orientations with different levels of interaction with the membrane: the parallel and the perpendicular mode [Figure 2(a) and (b), respectively]. The parallel mode [Figure 2(a)] engages the membrane-binding sites of all subunits of the hexamer to interact with the membrane simultaneously. In particular, the N-terminal residues of the protein interact with high propensity with the bilayer in this mode [Figure 2(c)]. In this mode, connection of different lipidic structures can be mediated by the hexamer [Figure 2(a)]. On the other hand, in the perpendicular mode only a few subunits interact with the bilayers [Figure 2(b)]. This incomplete membrane association suggests the perpendicular mode as an intermediate state before full association in the parallel mode. In all simulations, the central pore of the SP-B hexamer is filled with lipids, which is indicated by the increased lipid contact occupancy of the residues close to the center of the hexamer [Figure 2(c)].

The lipid contact occupancy plot in Figure 2(c) shows that the central pore, in particular, strongly supports lipid interactions in all lipid types. These interactions also include lipid insertion into the lipid-binding pockets in the functional dimers. These pockets can fully shield the phospholipid acyl chains from the polar aqueous environment as they are transferred through the protein. The simulations show that the lipids can be fully or partially enclosed in the cavity (Figure S7). In the partial enclosure, either one acyl chain or the head group of a phospholipid is inside the lipid-binding cavity. CHOL appears as the most common lipid to occupy the lipid-binding cavity and the central cavity as a whole, and this holds for all lipid compositions (Figure S8). Unlike phospholipids, which also interact with the N-terminal residues, CHOL interacts only with the central pore residues [Figure 2(c)]. This observation suggests that in SP-B, the lipid-binding cavity is not specific to phospholipids but can also bind CHOL (Figure S8).

Effect of POPG on the interaction of the SP-B hexamer with surfactant membranes

To study the effects of POPG on the binding mechanism and orientation of the SP-B hexamer, we simulated the spontaneous membrane adsorption of SP-B by initially placing it in the parallel orientation away from the bilayers with and without PG (PHYSIOL

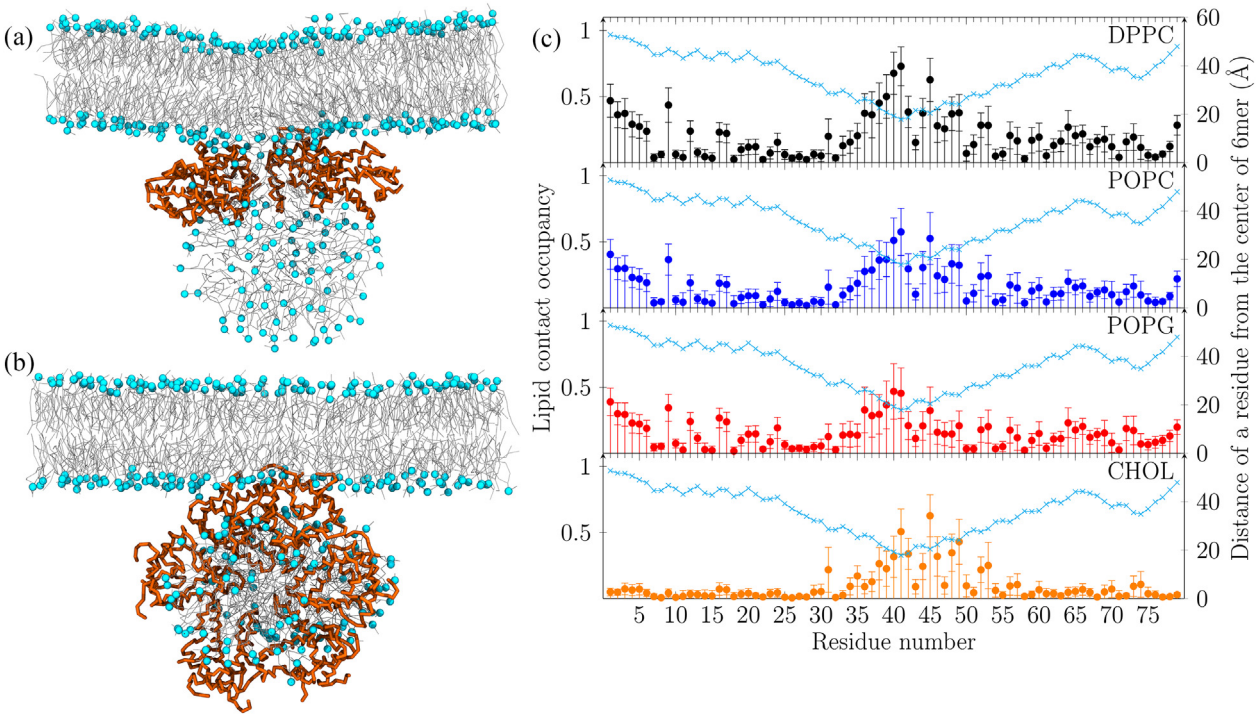

Figure 2. The membrane-binding modes and lipid–protein interactions in the SP-B hexamer. Representative snapshots with the hexamer in the parallel (a) and perpendicular (b) membrane-binding modes are shown. The snapshot in (a) also represents a configuration where the hexamer connects two lipidic structures, a bilayer and a micelle. (c) The lipid contact occupancy of each residue in the simulations. The contact occupancies are calculated from the self-assembly simulations performed with the PHYSIOL lipid composition (interaction cutoff 6 Å). The data are averaged over all monomeric units in the hexamer and all relevant simulations, with the bars showing the standard deviation. The blue line shows the distance of each residue from the central pore to indicate its relative position in the hexamer.

Table 1. The lipid compositions (in units of mol-%) used in this study

System	DPPC	POPC	POPG	CHOL
DPPC-CHOL	90			10
EQUI	25	25	25	25
NoPG	50	40		10
NoCHOL	55.6	27.7	16.7	
PHYSIOL	50	25	15	10

DPPC-CHOL" consists of DPPC and CHOL. "EQUI" refers to an equimolar mixture of the four different lipid components: DPPC, CHOL, POPC, and POPG. "NoPG" has no PG, "NoCHOL" has no CHOL, and "PHYSIOL" describes a physiological mixture in terms of these four lipids.

and NoPG lipid compositions, Table 1; see Methods: Bilayer simulations). The NoPG composition, used as a control here, maintains the same ratio between saturated and unsaturated phospholipids as in the PHYSIOL composition. In this manner, all other membrane properties were kept largely constant, allowing us to explore the effect of electrostatic protein–lipid interactions on membrane binding. Our simulations showed that POPG has a substantial effect on the rate of adsorption, affinity for membrane binding, and the orientation of the SP-B hexamer on membranes.

POPG affects the rate of adsorption and initial binding (Figure 3) of the SP-B hexamer on PSurf membranes. Based on the binding of the first dimer with the membrane in 24 repeats per composition (40 μs each repetition), adsorption to the PHYSIOL and NoPG bilayers takes on average 1.68 (±0.41) and 6.85 (±1.11) μs (±SE), respectively. Here, the comparison of the binding times is justified, since the protein is in all simulations initially in the same orientation and placed at the same distance (9 nm) away from both periodic images of the bilayer. Based on these results, the electrostatic interactions between SP-B and the anionic lipids (PHYSIOL) speed up the binding process roughly by a factor of 4 compared to a PG-free membrane (NoPG) when using the standard MARTINI force field [46,48,49].

The PSurf lipid composition affects the membrane-binding strength of SP-B. Interestingly, the membrane binding proceeds by sequential binding of functional dimers in a discrete manner as can be seen in the gradual stepwise increase in the number of contacts between the protein and the membrane lipids (Figure 3). In the presence of PG, the hexamer can achieve binding with up to three dimeric units, with a majority of simulations ending with two dimers bound within the time scale of the simulations (Figures 3 and 4). However, in the absence of PG, the protein binds with only one dimer, with only a few repeats capturing two-dimer binding (Figure 3). The one-dimer-bound state results in the previously discussed perpendicular orientation of the protein [Figure 4(a)]. Overall, the number of membrane-bound dimers fluctuates during the course of the

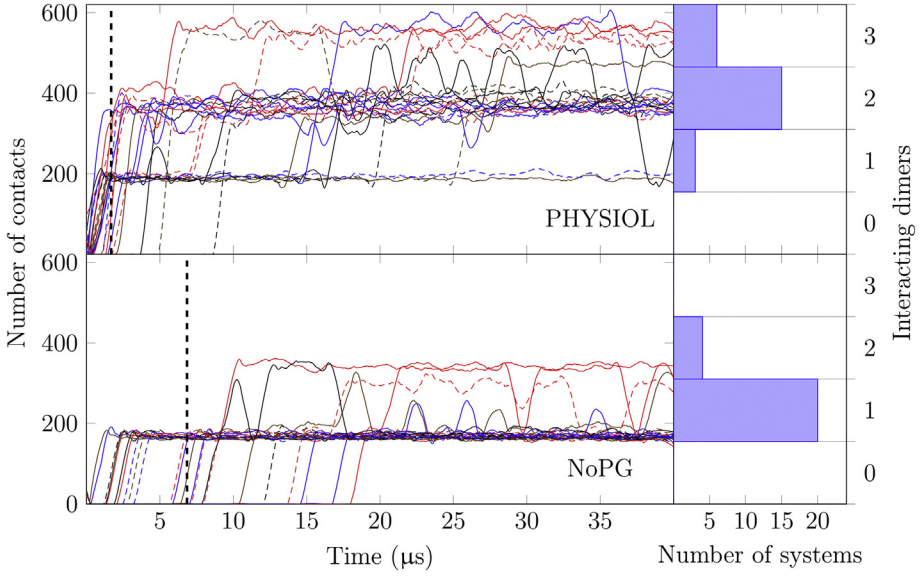

Figure 3. The rate of spontaneous membrane adsorption of SP-B. The number of contacts between the protein and the membrane is shown as a function of time for each simulation repeat for the PHYSIOL (top left) and NoPG (bottom left) lipid compositions. The average time required for the binding [1.68 (±0.41) μs (PHYSIOL) and 6.85 (±1.11) μs (NoPG), average (±SE)] is indicated by vertical dashed lines. The bar plots show the number of simulations in which a certain number of dimers (1–3 out of 6) is bound to the membrane at the end of the simulations, calculated based on the average number of contacts during the last 500 ns of the simulations for the PHYSIOL (top right) and NoPG (bottom right) lipid compositions.

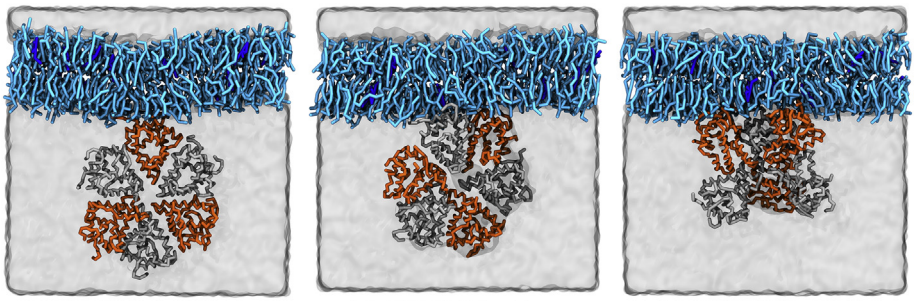

(a) NoPG, 40 μs (b) PHYSIOL, 40 μs (c) PHYSIOL, 40 μs

Figure 4. The SP-B hexamer adsorbs to the surface of membranes. The lipid composition of the membrane affects the rate and the strength of membrane binding, with SP-B binding faster and stronger with membranes containing POPG. (a) In the NoPG lipid composition, the SP-B hexamer binds preferably with only one dimer to the bilayer. (b, c) In the PHYSIOL lipid composition, the SP-B hexamer binds with two or three dimers. The electrostatic interactions between the negatively charged lipids and the positively charged residues in the membrane-binding face of SP-B have a significant effect on the binding process.

simulations. Although partial unbinding events do occur in both lipid compositions, after the initial binding, SP-B never desorbs completely from the membrane surface. More partial unbinding events occur in the NoPG systems where the electrostatic interactions between SP-B and the membrane are not as significant as in the PHYSIOL composition.

The perpendicular membrane-binding mode of SP-B is an intermediate step before full attachment to PSurf membranes. Shorter simulations with the improved polarizable MARTINI water model [47] with Particle-Mesh-Ewald (PME) electrostatics showed complete and successful SP-B membrane adsorption to be based on the parallel membrane-binding mode (see discussion in Section S2.2 in the SI). The parallel membrane binding of the SP-B hexamer also promotes lipid protrusions into the central pore of the ring (Figure S9).

Interaction of SP-B hexamers with lipid monolayers

To get better insight into the molecular mechanism of SP-B at the air–water interface, we investigated how SP-B hexamers interact with lipid monolayers. To construct these systems, we took advantage of the information provided by the self-assembly and bilayer simulations discussed above. Accordingly, we placed the SP-B hexamer in the parallel orientation, sandwiching it between two monolayers (for details, see Methods: Monolayer simulations).

In all systems considered, the SP-B hexamer causes lateral reorganization of the surfactant lipids (Figures 5 and S11–S15). The general trends are most clearly seen in the PHYSIOL lipid composition discussed below (Figure 5). The simulations suggest that both POPG and CHOL have distinct, functionally relevant, high-affinity interaction sites in the SP-B hexamer. At the same time, DPPC or palmitoyloleoylphosphatidylcholine (POPC) do not show any specific preference for SP-B. However, as further discussed in the next section, the effect of the SP-B hexamer on the different surfactant lipid species depends on the overall lipid composition and the average area per lipid (APL) of the monolayers it is in contact with.

POPG has two high-affinity interaction sites, one at the Principal Interface 1 and another at the Principal Interface 2 [Figures 1(f) and 5]. The first high-affinity POPG interaction site in the structure of the SP-B hexamer is at the Principal Interface 1 (Figures 5 and S11). The positively charged R36 at the membrane-perturbing site generates a POPG interaction hotspot in and around the central pore of the ring structure. The acyl chains of POPG molecules face toward the center of the ring [Figures 6(c) and S7]. At the Principal Interface 2, POPGs are located around the membrane-binding sites of SP-B, or more precisely, mainly interacting with the positively charged N- and C-terminal residues in helix 1 (R12, K16, and R17) and helix 4 (R72) (Figure 8).

CHOL has two main high-affinity interaction sites at the Principal Interface 1 (Figures 5 and 6). The first high-affinity interaction site is at the opening of the central pore of the SP-B hexamer ring [Figure 6(a)] and the second one inside the lipid-binding cavities between the non-covalently bound adjacent dimers [Figure 6(b)]. In the first interaction site, CHOL occupies either the opening of the lipid-binding cavity of the functional dimers near the central pore, or the small groove formed between the helices of two covalently bound SP-B monomers in the central pore [Figure 6(a)]. The first CHOL-binding site is highly conserved in all the six dimers in the SP-B hexamer structure and is seen at the Principal Interface 1 in Figure 5 as the six highly conserved interaction sites in the center of the protein ring. In the second interaction site, CHOL occupies the lipid-

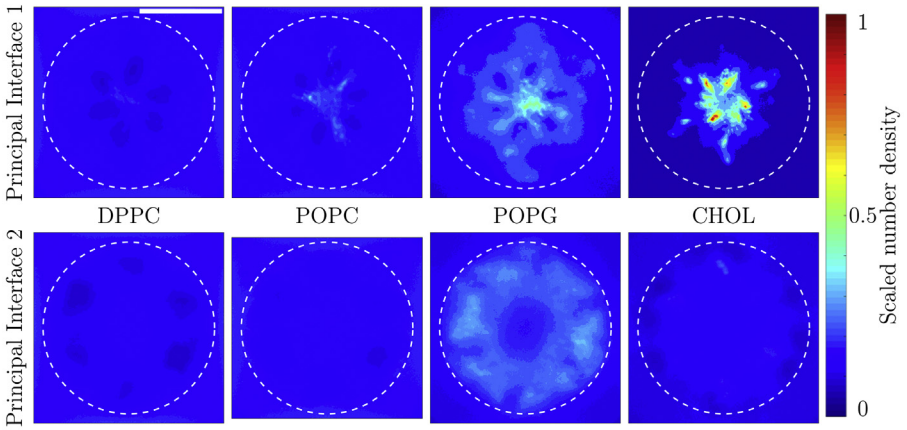

Figure 5. Lateral lipid reorganization in PSurf monolayers caused by the SP-B hexamer in the PHYSIOL lipid composition. The SP-B hexamer is in the middle of each image lying along the membrane plane (see POPG as an example). The two-dimensional scaled number densities for each lipid type are shown as heat maps. Results shown here have been averaged over 12 simulation repeats at the APL of 55.0 Å^2, normalized by the relative lipid composition. The scale bar (upper left panel) equals to 5 nm. The position and average size of the SP-B hexamer (10.4 nm) are indicated by a dashed circle.

binding cavities [Figure 6(b)] and at the same time blocks the cavity from other lipids. Preference for either high-affinity CHOL interaction site can change between the two states within the same simulation.

The occupancy of the high-affinity CHOL interaction sites depends on the lipid composition, APL of the monolayers, and the conformation of the protein. The first high-affinity CHOL interaction site in the central pore can be seen in the PHYSIOL lipid composition at both studied APLs (Figures 5 and S11). At the lower APL of 55 Å^2, CHOL is preferably in the central pore, whereas at 57.5 Å^2, CHOL alternates more often between both interaction sites. Indeed, in the PHYSIOL lipid composition, CHOL occupies interchangeably either of the high-affinity interaction sites, whereas in the NoPG lipid composition, CHOL is found only in the second interaction site, that is, inside the lipid-binding cavities (Figures S14–S15). In the PHYSIOL lipid composition, the combined effect of CHOL and POPG seems to result in more extensive monolayer perturbations (discussed in the next section), which we conclude to partly result from the small differences in the orientation of the dimers with respect to the monolayers that results from interactions with POPG. The first CHOL interaction site in the central pore is preferred with larger monolayer perturbations.

Perturbation of lipid monolayers by SP-B hexamers

The SP-B hexamer causes spontaneous perturbations and protrusion of lipids upon interaction of the Principal Interface 1 with the monolayer surface (Figure 7). Lipids protrude from one of the monolayers into the hydrophobic central pore of the SP-B

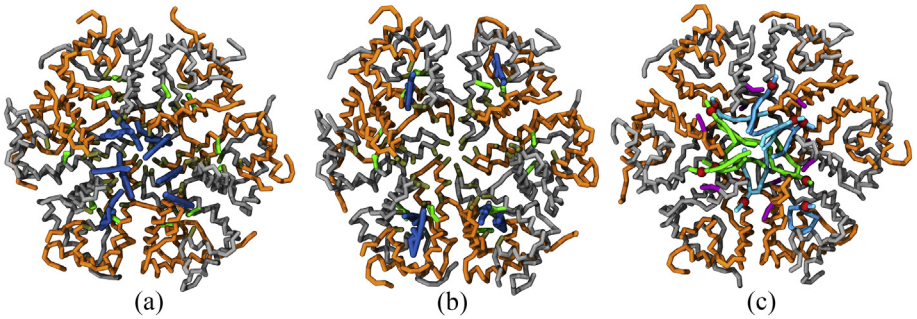

Figure 6. CHOL (blue) has two high-affinity interaction sites in the structure of the SP-B hexamer at the Principal Interface 1 shown in (a) and (b). (a) CHOL occupies the opening of the lipid-binding cavities or the crevice between the helices of two covalently bound SP-B monomers. (b) CHOL is inside the lipid-binding cavities of the SP-B hexamer in the second interaction site. (c) Phospholipids [POPG, green; phosphatidylcholines, cyan] tend to orient themselves with their headgroups (red) toward the R36 (magenta) near the entrance of the hydrophobic central pore.

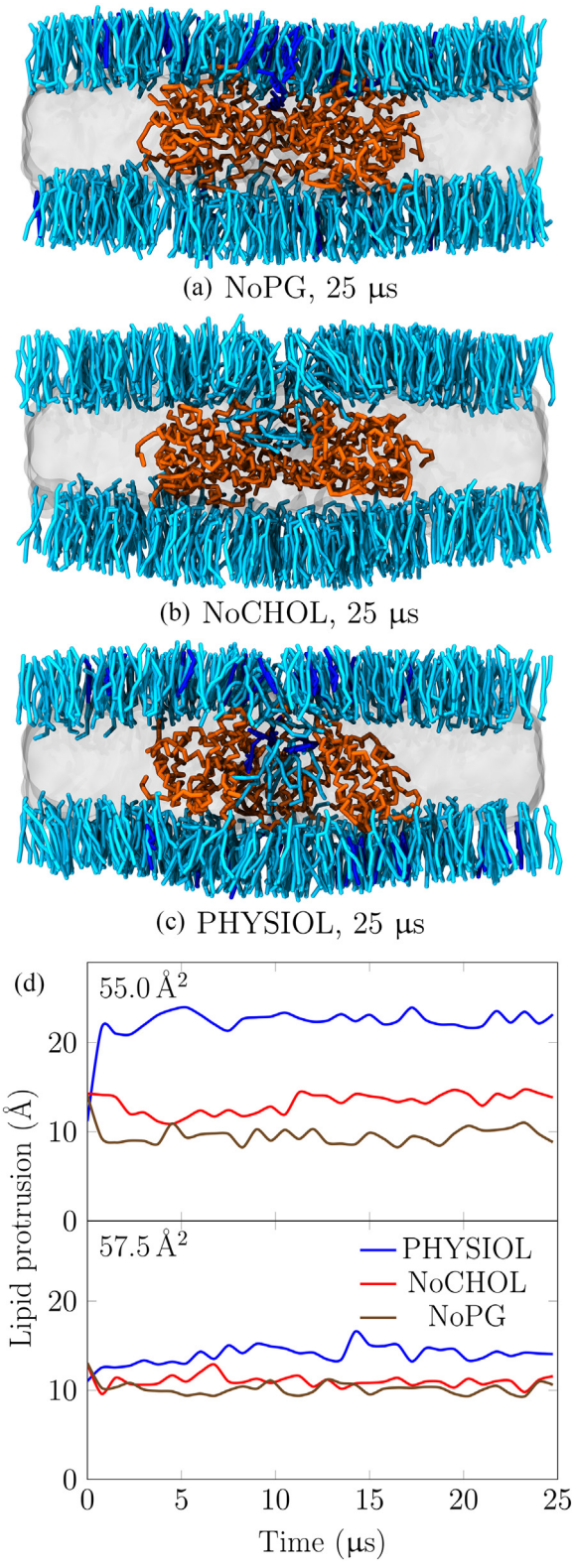

hexamer ring, forming a lipid neck largely spanning the SP-B hexamer. The monolayer perturbations occur only at the Principal Interface 1, where the previously discussed membrane-perturbing sites at the turn of the secondary structure (SP-$B_{36–45}$) are in contact with the membrane surface (Figure 1). The lipid perturbations depend on very small conformational changes in the protein structure upon membrane binding. The initial protrusion of lipids into the central pore occurs rapidly within the first 500 ns of the simulations after contact with the monolayer [Figure 7(d)]. The lipid neck that originates from these protrusions is not fully stable in the CG simulations. However, in complementary atomistic simulations (after fine-graining the present CG structures to atomistic resolution), we found the central cavity to be fully covered with lipids and the structure to remain stable (see the SI, Figure S16).

The extent of lipid protrusions into the central pore depends on the lipid composition and the APL of the monolayers (Figure 7). The level of membrane binding of SP-B and the relative orientation of the membrane-perturbing sites at the Principal Interface 2 with respect to the membrane surface also depend on the lipid composition. SP-B-induced monolayer perturbations are most significant in the PHYSIOL lipid composition, followed by the NoCHOL and NoPG compositions, respectively. POPG is the main cause for the notable change in the membrane binding and conformation of SP-B, thereby leading to the observed difference in the membrane-perturbing action of SP-B. In the PHYSIOL and NoCHOL lipid environments, the interaction of the positively charged membrane-binding residues of SP-B with POPG at the Principal Interface 2, and R36 on the other side, orients the dimers in the SP-B hexamer so that the membrane-perturbing sites at the Principal Interface 1 are in better contact with the lipids. This causes lipids to protrude into the central pore, and CHOL to bind into the high-affinity sites surrounding the inner edge of the central pore of the protein ring.

The average lipid protrusion is largest in the APL of 55.0 Å^2 PHYSIOL systems, reaching almost complete transfer of lipids through the central cavity of the protein in some of the systems (Figure 7). Generally, the effect of the APL on SP-B-induced lipid protrusion is most significant in the PHYSIOL

Figure 7. SP-B hexamer causes perturbations in surfactant monolayers upon interaction. (a, b) Lipid protrusions are minor in the NoPG and NoCHOL lipid compositions, respectively. (c) In the PHYSIOL lipid composition, where both CHOL and POPG are included, SP-B causes large lipid protrusions that largely span the central cavity. (d) Average lipid protrusion distances into the central pore of the SP-B hexamer in the PHYSIOL, NoCHOL, and NoPG lipid compositions at the APL of 55.0 and 57.5 Å^2.

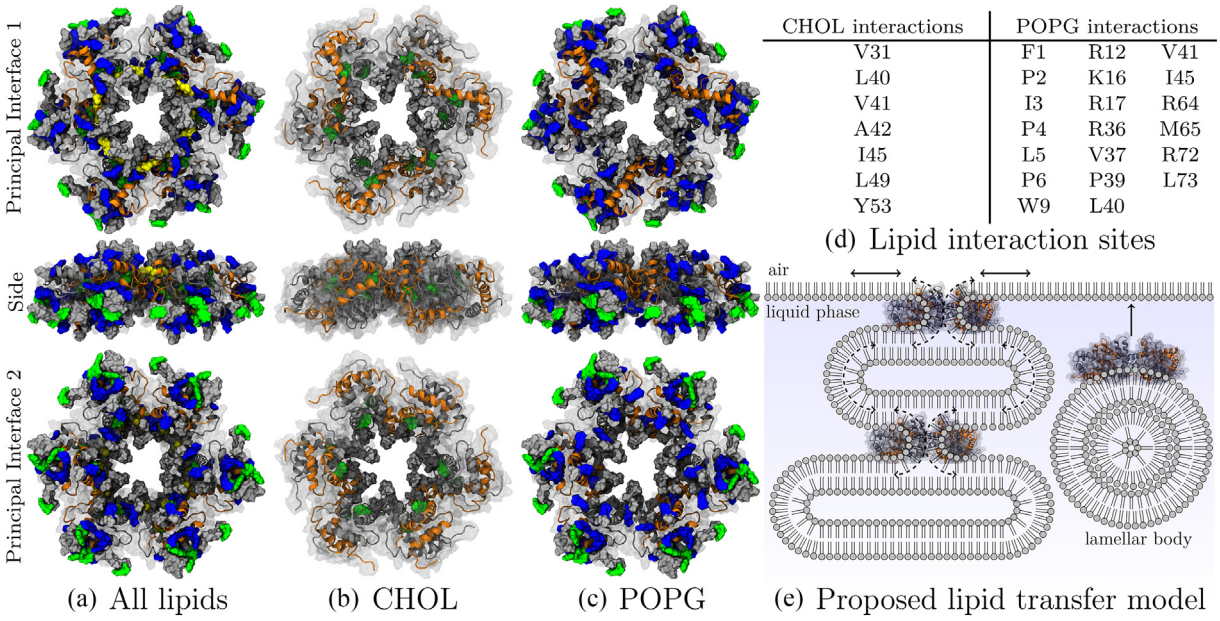

Figure 8. The main lipid interaction sites described in this study projected on the atomistic SP-B hexamer model and a proposed lipid transfer model for the supradimeric SP-B oligomers in PSurf membranes. (a) The most important membrane-binding residues with the highest lipid contact occupancies [threshold 0.5, Figure S8(a)] in the lipid self-assembly and monolayer simulations cover the membrane-binding sites and the central pore of the SP-B hexamer. (b, c) The identified CHOL-interacting residues, and the POPG-interacting residues, respectively, shown on the structure, and (d) the same residues listed. (e) Our results suggest that SP-B oligomers may bridge surfactant structures together through the hydrophobic central pore. Transfer of lipids would be mediated by the changes in the lateral pressure of the surfactant layers during compression–expansion cycles of the alveoli. The colors in (a–c) are set for hydrophobic residues (gray), positively (blue), and negatively (red) charged residues, aromatic residues (green), neutral residues (white), and cysteines (yellow).

systems. At the same time, in the NoPG systems, the difference in the APL (55.0 $Å^2$ *versus* 57.5 $Å^2$) does not affect the extent of lipid protrusion, which remains minimal during the 25-μs simulation. At 57.5 $Å^2$ in the NoPG and NoCHOL systems, SP-B causes only small lipid perturbations.

Discussion

The lipid self-assembly simulations with the SP-B hexamer show two main lipid-binding orientations at the surface of bilayers. The unifying feature with these two lipid-binding modes is the lipid-filled central cavity of the SP-B hexamer. Interestingly, the self-assembly simulations show that in the parallel mode, the protein can bridge a bilayer to a secondary lipid assembly, such as a micelle [Figure 2(a)] or a small bilayer disc, by maintaining a continuous lipid phase between them. This feature is further supported by the original idea by Olmeda *et al.* [35] and Hobi *et al.* [14] that by binding membranes in the parallel mode, SP-B oligomers can connect lipidic structures and facilitate lipid transfer between them through its hydrophobic central pore. Previous computational studies have shown [43,45,50] the role of SP-B monomers and dimers in lipid transfer between lipid reservoirs and surfactant membranes through similar lipid necks. Furthermore, oligomerization of SP-B in the presence of POPG has been shown to further enhance its activity in lipid transfer [19]. Thus, the parallel membrane-binding orientation of the SP-B hexamer would better fit the previous experimental and computational findings.

SP-B is known to interact preferentially with anionic phospholipids, such as PG and phosphatidylinositol [17,18]. Indeed, the large net positive charge (+84) of the SP-B hexamer can explain this behavior [38]. How these interactions take place at the molecular level remains unclear, though, as does also their role in the function of SP-B. Experiments have shown that anionic lipids, such as POPG, could be essential for the adoption of the oligomeric organization of SP-B on surfactant membranes [19]. Our results are in line with these previous findings and clearly show that the presence of PG has an important role in SP-B interaction with the membrane, promoting and accelerating the binding of the protein and allowing the sequential attachment of dimers, which would result in a proper orientation of the complex parallel to the membrane.

The lipid self-assembly simulations of the SP-B hexamer result in two main membrane-binding orientations, the perpendicular and parallel mode. We note

that the simulations here with the standard MARTINI model do not systematically capture the formation of the fully parallel binding mode during the simulated 40 μs. Still the propensity of SP-B turning toward the parallel membrane-binding orientation in the PHYSIOL composition indicates that limitations in the electrostatics of the standard MARTINI model may cause inconclusive results. To this end, we ran three extra repetitions of equivalent binding simulations utilizing the improved polarizable water model [47] for MARTINI with the new-PME parameters (see discussion in the SI and Figures S9 and S10), since the combination of PME and the polarizable water model provide a proper description of long-range electrostatic interactions, including solvent screening. In these additional simulations, SP-B reached the parallel membrane-binding orientation in all PHYSIOL systems (see Figure S9). In the NoPG systems, SP-B did not bind to the membrane within the 2.5-μs simulation, while in the PHYSIOL composition, the binding was almost instant (see Figure S10). Thus, we conclude that both the perpendicular and parallel membrane-binding modes are present in the standard MARTINI simulations, as we see in the self-assembly systems. The proper description of long-range electrostatics is needed to reach the parallel mode within reasonable simulation time, and this difference stresses the importance of electrostatic interactions in the binding process. Given that the parallel membrane-binding mode of SP-B is fully compatible with previous experimental observations [19,35], and also consistent with both the lipid self-assembly and adsorption simulations, there is sufficient evidence to conclude that the SP-B hexamer is found in PSurf membranes in the parallel binding orientation. The perpendicular binding occurs in the simulations as an intermediate state before full incorporation to the membrane surface.

The positions of the most important lipid-binding residues at both Principal Interfaces are further elucidated in Figure 8. In the present work, the high net charge of the Principal Interface 2 causes lateral reorganization in the membrane and a high local concentration of POPG around the SP-B hexamer, similar to the enrichment of negatively charged lipids near the protein observed in experiments [17]. Furthermore, POPG displaces other phospholipids around the SP-B hexamer. The high affinity of POPG to the Principal Interface 2, that is, the essential main experimentally observed membrane-binding face of SP-B [51–53], is evident in every system we explored with the PHYSIOL and NoCHOL lipid compositions (Figures 5 and S11–S13). Furthermore, at the Principal Interface 1, R36 is the most important residue that binds with POPG. The biological function of R36 could be related to its high affinity to the anionic PSurf lipid species. Thus, R36 could dock the SP-B hexamer rings to a second membrane through electrostatic interactions with anionic lipids and thus allow the transfer of lipids between the interconnected surfactant membranes through the ring-like oligomer structure.

Experiments have shown [8,10,28] that elevated levels of CHOL may cause surfactant inhibition, while physiological levels of CHOL have no detrimental effects on the function of the PSurf or SP-B. Indeed, SP-B in the presence of CHOL has been shown to somehow improve the biophysical properties of the PSurf and its clinical replacements [54–56]. The potential interaction between SP-C and CHOL in surfactant membranes has been previously addressed [39,57–60], pointing to a potential role of this protein in ensuring a proper surfactant distribution and metabolism of CHOL. A functional cooperation of this protein with SP-B in membranes containing CHOL [61] has been reported. However, to our knowledge, our results provide the first indication of specific CHOL-binding sites in the functional structures of SP-B oligomers. These specific interactions could also be important for the activity of SP-B and should be further characterized in future studies.

The fusogenic, lytic, and surface tension lowering functions of SP-B have been determined to be predominantly caused by the N-terminal half of the protein, which includes helices 1 and 2 (SP-$B_{8–22}$ and SP-$B_{26–35}$, respectively) [51]. In the same study, the C-terminal half of SP-B with helices 3 and 4 (SP-$B_{42–63}$ and SP-$B_{68–74}$, respectively) had significantly lower activities in all of these functions. Our results indicate a possible fusogenic and/or lytic domain at the bend between helices 2 and 3 (SP-$B_{36–45}$). In our simulations, this site is essential for the membrane-perturbing function of the SP-B hexamer. Moreover, our simulations captured membrane insertion of the disulfide-bridged dimers. The insertion and subsequent oligomerization of the disulfide-bridged SP-B dimers on surfactant membranes (Figure S6) can potentially induce the formation of proteolipid pores or invaginations in bilayers observed in experiments [62,63].

A recent study by Hobi *et al*. suggested that the release of the surface-active phospholipids to the air–liquid interface would be driven by a high internal pressure of the lamellar bodies and activation of the protein upon contact with air [14]. Similarly, the lateral surface pressure changes of the PSurf during the compression–expansion cycles of breathing have been suggested to promote reversible squeeze-out and re-extension of lipids mediated by SP-B [4,9,23]. Small alternating conformational transitions in the SP-B tertiary structure upon contact with the air–water interface [14,35] or upon the changes in lateral surface pressure of the PSurf monolayer during the breathing cycle could activate SP-B oligomers. In this way, SP-B would allow rapid flow of lipids into the alveolar surface in the spreading and re-extension phases and squeeze-out of lipids from the surface during sufficient

compression [Figure 8(e)]. Our observed ability of SP-B hexamers to form lipid necks protruding from monolayers or bilayers could be also related to the reported ability of the protein to promote lipid phases with negative curvature in the presence of anionic phospholipids [64,65].

All in all, these results help to understand the molecular mechanism of SP-B oligomers in the transfer of surface-active phospholipids from PSurf membranes into the respiratory surface. Our results support a model in which SP-B activity in lipid transfer across the central cavity depends greatly on the monolayer compression associated with lateral pressure during the respiration cycle, and the changes in the conformation of the protein. Our results further suggest that the lipid transfer mediated by SP-B oligomers would occur specifically through the hydrophobic central pore [Figure 8(e)]. We note that in this study we only considered hexamers, and higher-order oligomers are likely to exhibit somewhat different properties for lipid transport and membrane-perturbing properties. A larger number of dimers would essentially allow for more orientational flexibility around the inter-chain disulfide bridge, and thus more deformability, shape variation, and asymmetry. Indeed, there may be a functional mixture of various oligomeric sizes as different oligomers with somewhat different properties can work in synergy.

Conclusions

Using extensive CG-MD simulations, we investigated how the SP-B complex (in a number of oligomeric states) interacts with PSurf membranes, and how the specific protein–lipid interactions associated with membrane binding are related to the molecular mechanism of its lipid transfer function.

We found two potential conserved lipid interaction sites in the structure of the SP-B hexamer: the first corresponding to the membrane-binding residues located in the N-terminal half of SP-B, and the second one near the bend between helices 2 and 3 (SP-$B_{36–45}$). The first lipid interaction site seems essential for the correct binding and orientation of the protein with the PSurf membranes through hydrophobic and electrostatic interactions of the membrane-binding residues. The second lipid interaction site shows significant membrane-perturbing functions in the SP-B hexamer, which to our knowledge has not been demonstrated in previous studies.

Our results indicate that in particular PG and CHOL have a significant role in the function and efficiency of SP-B. As to PG, it is relevant to first bring out that SP-B has a high net positive charge with many functionally essential positively charged membrane-binding residues that affect the activity of the SP-B hexamer by causing small changes in the binding orientation of the dimers with respect to the negatively charged PSurf membrane surface. Next, regarding CHOL, our results suggest two novel high-affinity CHOL-binding sites in the structure of the SP-B hexamer. The position of the first CHOL-binding site is near the opening of the hydrophobic central pore, while the second one is inside the lipid-binding cavities of the SP-B hexamer.

Based on our studies, we find that the SP-B hexamer induces the formation of membrane perturbations in PSurf through the central pore of the oligomer ring. The lipid-binding cavities between the adjacent disulfide-bridged SP-B dimers are important for this mechanism as they can reversibly enclose lipids inside. Lipid protrusions through the central pore of the SP-B hexamer could facilitate the connection and rapid lipid transfer between different surfactant structures.

Methods

The SP-B models and the simulation protocols

All CG-MD simulations (described below) used in this study were initiated from the following atomistic models of different oligomeric states of SP-B. The description below regarding the construction of the SP-B model is illustrated in Figure 1.

The SP-B functional dimer models

The homology models of SP-B functional dimers were obtained as previously described [35]. As in the dimeric saposin B crystal structure (PDBID: 1N69) [36] used as the template, the SP-B functional dimer is modeled in two conformations (open and closed), and features a lipid-binding site between the monomers. In the simulations, we used the closed version of the dimer (see Section S2.1 in SI), which corresponds to the closed AB dimer of saposin B [36]. Further, there is reason to stress that while there are several possible templates in the saposin family, we decided to use 1 N69 because SP-B is known to be functional as a dimer, 1 N69 (unlike many other templates) describes the dimeric state, and it has been postulated that oligomerization of dimers is necessary for the ring-like supramolecular organization.

The SP-B supradimeric oligomer models

The functional dimer homology model was subjected to symmetric rigid docking [66] using the Rosetta software suite [67] to generate the ring-shaped supradimeric oligomer models of various sizes that conform to the criteria proposed [35]. Specifically, the higher-order oligomer models were ensured to (i) contain the SAPLIP-like functional dimer as a

structural unit in an either open or closed conformation, (ii) have an inter-dimeric interface that can accommodate an inter-chain disulfide bridge between C48 residues and salt-bridges between respective E51 and R52 residues, and (iii) have the putative lipid-binding site of each functional dimer facing toward the center of the ring.

The SP-B dimer homology models extracted from the Olmeda *et al*. oligomer models [35] were first relaxed using the fast-relax protocol [68]. Then, symmetric docking [66] was performed with appropriate cyclic symmetry definitions for the desired number of dimers. During symmetric docking, the distances between neighboring C48 residues were restrained using the "flat harmonic" restraint type, with the center of restraint, the tolerance, and the width parameters set to 2.0, 1.8, and 0.5 Å/$\sqrt{\text{REU}}$, where REU stands for the Rosetta Energy Unit.

The models were later sorted based on their total score and filtered. Top scoring models were first clustered using Calibur [69]. The cluster centers that satisfied the conditions (ii) and (iii) based on visual inspection using visual molecular dynamics [70] were selected for the next steps. These structures were further subjected to the fast-relax protocol [68], where the intra- and inter-chain disulfide bridges were set explicitly to optimize the side chain geometries. In all stages of modeling, the talaris2014 score function [71] was employed.

The exact number of dimers in the multidimeric SP-B complex is not known [35,37]. To account for this diversity and uncertainty, in our simulation work, we focused on hexamers (see comparison of oligomer sizes in Figure S17). This decision was based on both feasibility of the structure, the size of the simulation systems, and the point that hexamers fit well into the EM density as described further [35].

The disulfide-bridged dimer models

The models of the disulfide bridged dimer were generated by extracting two neighboring monomers connected by the interchain disulfide bond at C48 from the hexameric oligomer constructed as described above.

CG-MD simulations

CG-MD simulations of the aforementioned oligomeric states of SP-B were performed in three different environments: lipid dispersion (self-assembly), bilayers, and monolayers (see below for detailed descriptions). Table 1 lists all studied lipid compositions.

Simulation protocols

The CG non-polarizable Martini model version 2.2 [46,48,49] with the "newRF" parameters as described [72] was employed, unless mentioned otherwise. The CG protein models were built from the aforementioned all-atom models using martinize.py (version 2.2) [46]. All CG protein models used in the simulations described below were based on the closed SP-B conformation. The protonation state of each residue was assigned based on its pK_a in aqueous solution at pH 7. An elastic network with the default options [73] was used to preserve the secondary and tertiary structures of the proteins. More precisely, the elastic bond force constant was 500 kJ mol^{-1} nm^{-2} and the cutoff distance (RC) was 0.9 nm. For supradimeric oligomers, elastic network bonds between the subunits connected by the inter-chain disulfide bridges were removed to allow reorientation of the subunits and to account for some conformational flexibility of the oligomers. The elastic network is used to preserve higher-order structure of proteins in the Martini model [46], but it also restricts the protein from changing conformation from, e.g. between the suggested open and closed conformation of SP-B. We concentrated on the closed conformation, as discussed above.

All simulations were performed using the Gromacs 5.1.x software package [74] with an integration time step of 25 fs. Coulombic interactions were calculated using the reaction-field algorithm [75] with $\varepsilon_r = 15$ and $\varepsilon_{rf} = \infty$. The Verlet [76] cutoff scheme was employed for the non-bonded interactions with an LJ cutoff (for Lennard–Jones interactions) of 1.1 nm. The temperature was controlled using the stochastic velocity rescaling thermostat [77] with the protein, lipids, and solvent (water and ions) coupled to separate heat baths each at 310 K with a time constant of 1.0 ps. For pressure coupling, the Parrinello–Rahman barostat [78] was employed, unless otherwise stated. The self-assembly and the bilayer simulations were performed in the NpT ensemble with isotropic and semi-isotropic pressure coupling, respectively, with the reference pressure set to 1 bar and the time constant to 12 ps. The monolayer simulations were performed in the NVT ensemble. Periodic boundary conditions were used in all dimensions.

The refined polarizable Martini water model with the "newPME" parameters as described [47] (together with PME) was used in a subset of the bilayer simulations. This improved water model with the new parameters suited for PME electrostatics provides more precise long-range electrostatics in Martini simulations. The newPME parameters are identical to the newRF ones, with the exception of using the smooth PME method [79]. As with the standard polarizable Martini water model [80], $\varepsilon_r = 2.5$. The LINCS [81] algorithm was used to constrain all bond lengths within the water beads.

Lipid self-assembly simulations

Separate lipid self-assembly simulations were performed to investigate the spontaneous assembly of lipids around all SP-B models: SP-B disulfide-

bridged dimer, SP-B functional dimer, and the SP-B hexamer. For each protein, four different lipid compositions were considered (see Table 1): DPPC-CHOL, equimolar (EQUI), no CHOL (NoCHOL), and physiological (PHYSIOL). The simulations were initiated with lipids placed randomly in the simulation box with the protein in the center. No lipids were placed in the putative lipid-binding pockets of the SP-B functional dimer or the SP-B hexamer prior to any of the simulations. The number of lipids for self-assembly was chosen based on the size of the protein (300, 600, 600, and 1100, respectively). The systems were solvated with 20 water beads per lipid, except for the hexamer system, where 30 water beads per lipid were added. Ions were added to attain a physiological salt concentration of 0.15 M of NaCl in addition to those needed for neutralizing the systems. For each lipid–protein composition, 24 self-assembly simulations, each 2.5 μs long, were performed (4 proteins × 4 lipid compositions × 24 × 2.5 μs = 960 μs in total). The self-assembly simulations were performed with isotropic pressure control. See Table S1 (in the SI) for the detailed composition of each system.

Bilayer simulations

First, a bilayer consisting of a total of 880 lipids with the PHYSIOL composition and 20 water beads per lipid was built using insane.py [82] and simulated for 20 ns. Using this configuration, another bilayer with the NoPG composition was prepared by substituting the POPG molecules in the PHYSIOL bilayer with POPC. Both bilayers were then equilibrated for another 20 ns. SP-B hexamer was next added to each bilayer system such that its distance to each leaflet was 9 nm and the axis of its central pore was parallel to the membrane normal. After solvation (~43 water beads per lipid) and addition of neutralizing ions (see Table S2), the systems were energy minimized and equilibrated with the protein restrained for 20 ns. After equilibration, 24 repetitions were simulated for 40 μs each, using both PHYSIOL and NoPG compositions (2 × 24 × 40 μs in total). The production simulations of the bilayer systems were performed with semi-isotropic pressure control.

The same equilibrated bilayer constructions with the SP-B hexamer, as described below, were used as a basis of the polarizable water model systems. The standard water beads were replaced with the three-point water beads, and the systems were then minimized and equilibrated for 20 ns, as described above. After equilibration, three repetitions were simulated for 2.5 μs each, using both PHYSIOL and NoPG compositions.

Monolayer simulations

The interaction of the SP-B hexamer with monolayers was studied using three different lipid compositions (PHYSIOL, NoPG, NoCHOL; see Table 1). The monolayers were prepared from bilayers of the same composition by separating the leaflets. The box dimension along the monolayer normal (*z*) was set to 20 nm to prevent interactions through the vacuum, which was used to mimic the air–water interface of the alveoli. To maintain the vacuum between the monolayers, all monolayer simulations were performed in the NVT ensemble with the box dimensions along the membrane plane set to achieve two different initial APL values for each lipid composition: 55 or 57.5 $Å^2$. The protein was added to the monolayer systems such that the axis of the central pore was parallel to the monolayer normal and the protein was in contact with both monolayers. To investigate the effect of hydration (i.e. monolayer distance), we placed a different number of water molecules between the leaflets: 4000, 4500, 5000, or 5500 water beads for the APL of 55 $Å^2$, and 4500, 5000, 5500, or 6000 water beads for the APL of 57.5 $Å^2$. For each system, three repetitions were run for 25 μs (75 μs for each lipid composition and number-of-water-beads combinations; 1800 μs in total; see Table S3).

Analysis

Residue-specific lipid interaction

The lipid contact occupancy with SP-B was calculated by counting the times a given type of lipid was within a distance of 6 Å from a specific residue in a trajectory, and then normalized by the number of each repeating residue and number of frames. For the dimer structures, the residues repeat twice, while in the SP-B hexamer, each residue repeats 12 times. The first 500 ns of the trajectories was omitted from the analysis. The distance of a residue from the center of the SP-B hexamer was calculated from the structure shown in Figure 1(g) and is depicted to indicate the approximate relative position of each residue in SP-B.

Rate of membrane adsorption

The number of contacts between the protein and the lipids was calculated using the gmx mindist tool with a cutoff of 6 Å. The time required for membrane binding was determined based on the number of contacts, and calculated by averaging over all 24 repetitions in both lipid compositions. The last 500 ns of the trajectory was used to determine the number of dimers in the hexamer in contact with the membrane. One dimer corresponds to approximately 200 protein–lipid contacts.

Lateral lipid reorganization

The two-dimensional number density for each lipid type in the monolayer systems was calculated with

the gmx densmap tool. The first 500 ns of the trajectories was omitted from the analysis. Results were normalized per relative lipid composition and averaged over 12 parallel repetitions at a given APL.

Lipid protrusion

The protrusion of lipids from the monolayer into the central pore of the hexamer ring were evaluated by calculating the difference in the *z* direction between the lipids in or near the central pore and the lipids around the protein. Results were averaged over the systems with the same lipid composition at both APLs.

CRediT authorship contribution statement

Juho Liekkinen: Methodology, Software, Validation, Formal analysis, Investigation, Data curation, Writing - original draft, Visualization.**Giray Enkavi:**Methodology, Software, Supervision, Validation, Writing - original draft.**Matti Javanainen:**Methodology, Supervision, Validation, Writing - review & editing.**Barbara Olmeda:**Conceptualization, Writing - review & editing. **Jesús Pérez-Gil:**Conceptualization, Writing - review & editing, Funding acquisition.**Ilpo Vattulainen:**Conceptualization, Validation, Resources, Writing - original draft, Supervision, Project administration, Funding acquisition.

Acknowledgments

We thank CSC—IT Center for Science (Espoo, Finland) for computing resources. We also thank the Sigrid Jusélius Foundation, the Academy of Finland (Centre of Excellence program), and the Helsinki Institute of Life Science Fellow program for financial support (I.V.). M.J. thanks the Emil Aaltonen Foundation for financial support. B.O. and J.P.-G. also acknowledge financial support from The Spanish Ministry of Science and Universities (RTI2018-094564-B-100) and the Regional Government of Madrid (P2018/NMT-4389).

Appendix A. Supplementary Data

Supplementary data to this article (further details on simulation setup and simulation methodology, and additional results from simulations) can be found online https://doi.org/10.1016/j.jmb.2020.02.028.

Received 30 October 2019;
Received in revised form 22 February 2020;
Accepted 24 February 2020
Available online 2 March 2020
Keywords:
pulmonary surfactant;
protein–lipid interactions;
SP-B;
molecular dynamics simulation

†Principal corresponding author.

Abbreviations used:
SP-B, surfactant protein B; PSurf, pulmonary surfactant; CHOL, cholesterol; SP, surfactant protein; DPPC, dipalmitoylphosphatidylcholine; PG, phosphatidylglycerol; SAPLIP, saposin-like protein; EM, electron microscopy; CG, coarse-grained; MD, molecular dynamics; POPC, palmitoyloleoylphosphatidylcholine; POPG, palmitoyloleoylphosphatidylglycerol; PI, phosphatidylinositol; APL, area per lipid.

References

[1] J. Goerke, Pulmonary surfactant: functions and molecular composition, Biochim. Biophys. Acta Mol. Basis Dis. 1408 (1998) 79–89.
[2] J. Pérez-Gil, K.M.W. Keough, Interfacial properties of surfactant proteins, Biochim. Biophys. Acta Mol. Basis Dis. 1408 (1998) 203–217.
[3] J. Pérez-Gil, Structure of pulmonary surfactant membranes and films: the role of proteins and lipid–protein interactions, Biochim. Biophys. Acta Biomembr. 1778 (2008) 1676–1695.
[4] A.G. Serrano, J. Pérez-Gil, Protein–lipid interactions and surface activity in the pulmonary surfactant system, Chem. Phys. Lipids 141 (2006) 105–118.
[5] E. Lopez-Rodriguez, J. Pérez-Gil, Structure–function relationships in pulmonary surfactant membranes: from biophysics to therapy, Biochim. Biophys. Acta Biomembr. 1838 (2014) 1568–1585.
[6] S. Orgeig, P.S. Hiemstra, E.J.A. Veldhuizen, C. Casals, H.W. Clark, A. Haczku, et al., Recent advances in alveolar biology: evolution and function of alveolar proteins, Respir. Physiol. Neurobiol. 173 (2010) S43–S54.
[7] C. Autilio, J. Pérez-Gil, Understanding the principle biophysics concepts of pulmonary surfactant in health and disease, Arch. Dis. Child. Fetal Neonatal Ed. 104 (2019) F443F51.
[8] Y.Y. Zuo, R. Veldhuizen, A.W. Neumann, N.O. Petersen, F. Possmayer, Current perspectives in pulmonary surfactant-inhibition, enhancement and evaluation, Biochim. Biophys. Acta Biomembr. 1778 (2008) 1947–1977.
[9] R. Wüstneck, J. Pérez-Gil, N. Wüstneck, A. Cruz, V.B. Fainerman, U. Pison, Interfacial properties of pulmonary surfactant layers, Adv. Colloid Interf. Sci. 117 (2005) 33–58.
[10] C. Casals, O. Cañadas, Role of lipid ordered/disordered phase coexistence in pulmonary surfactant function, Biochim. Biophys. Acta Biomembr. 1818 (2012) 2550–2562.
[11] R. Veldhuizen, K. Nag, S. Orgeig, F. Possmayer, The role of lipids in pulmonary surfactant, Biochim. Biophys. Acta Mol. Basis Dis. 1408 (1998) 90–108.
[12] J.B. de la Serna, S. Hansen, Z. Berzina, A.C. Simonsen, H.K. Hannibal-Bach, J. Knudsen, et al., Compositional and structural characterization of monolayers and bilayers composed of native

pulmonary surfactant from wild type mice, Biochim. Biophys. Acta Biomembr. 1828 (2013) 2450–2459.
[13] J.B. de la Serna, R. Vargas, V. Picardi, A. Cruz, R. Arranz, J. M. Valpuesta, et al., Segregated ordered lipid phases and protein-promoted membrane cohesivity are required for pulmonary surfactant films to stabilize and protect the respiratory surface, Faraday Discuss. 161 (2012) 535–548.
[14] N. Hobi, M. Giolai, B. Olmeda, P. Miklavc, E. Felder, P. Walther, et al., A small key unlocks a heavy door: the essential function of the small hydrophobic proteins SP-B and SP-C to trigger adsorption of pulmonary surfactant lamellar bodies, Biochim. Biophys. Acta, Mol. Cell Res. 1863 (2016) 2124–2134.
[15] J.B. de la Serna, J. Pérez-Gil, A.C. Simonsen, L.A. Bagatolli, Cholesterol rules: direct observation of the coexistence of two fluid phases in native pulmonary surfactant membranes at physiological temperatures, J. Biol. Chem. 279 (2004) 40715–40722.
[16] J.B. de la Serna, G. Orädd, L.A. Bagatolli, A.C. Simonsen, D. Marsh, G. Lindblom, et al., Segregated phases in pulmonary surfactant membranes do not show coexistence of lipid populations with differentiated dynamic properties, Biophys. J. 97 (2009) 1381–1389.
[17] E.J. Cabré, L.M.S. Loura, A. Fedorov, J. Pérez-Gil, M. Prieto, Topology and lipid selectivity of pulmonary surfactant protein SP-B in membranes: answers from fluorescence, Biochim. Biophys. Acta Biomembr. 1818 (2012) 1717–1725.
[18] J. Pérez-Gil, C. Casals, D. Marsh, Interactions of hydrophobic lung surfactant proteins SP-B and SP-C with dipalmitoylphosphatidylcholine and dipalmitoylphosphatidylglycerol bilayers studied by electron spin resonance spectroscopy, Biochemistry. 34 (1995) 3964–3971.
[19] M. Martínez-Calle, B. Olmeda, P. Dietl, M. Frick, J. Pérez-Gil, Pulmonary surfactant protein SP-B promotes exocytosis of lamellar bodies in alveolar type II cells, FASEB J. 32 (2018) 4600–4611.
[20] A. Cruz, L.A. Worthman, A.G. Serrano, C. Casals, K.M.W. Keough, J. Pérez-Gil, Microstructure and dynamic surface properties of surfactant protein SP-B/dipalmitoylphosphatidylcholine interfacial films spread from lipid–protein bilayers, Eur. Biophys. J. 29 (2000) 204–213.
[21] A. Cruz, L. Vázquez, M. Vélez, J. Pérez-Gil, Effect of pulmonary surfactant protein SP-B on the micro- and nanostructure of phospholipid films, Biophys. J. 86 (2004) 308–320.
[22] E.J. Cabré, J. Malmström, D. Sutherland, J. Pérez-Gil, D.E. Otzen, Surfactant protein SP-B strongly modifies surface collapse of phospholipid vesicles: insights from a quartz crystal microbalance with dissipation, Biophys. J. 97 (2009) 768–776.
[23] D. Schürch, O.L. Ospina, A. Cruz, J. Pérez-Gil, Combined and independent action of proteins SP-B and SP-C in the surface behavior and mechanical stability of pulmonary surfactant films, Biophys. J. 99 (2010) 3290–3299.
[24] L.M. Nogee, G. Garnier, H.C. Dietz, L. Singer, A.M. Murphy, D.E. DeMello, et al., A mutation in the surfactant protein B gene responsible for fatal neonatal respiratory disease in multiple kindreds, J. Clin. Invest. 93 (1994) 1860–1863.
[25] J.C. Clark, S.E. Wert, C.J. Bachurski, M.T. Stahlman, B.R. Stripp, T.E. Weaver, et al., Targeted disruption of the surfactant protein B gene disrupts surfactant homeostasis, causing respiratory failure in newborn mice, Proc. Natl. Acad. Sci. U. S. A. 92 (1995) 7794–7798.
[26] K.E. Greene, J.R. Wright, K.P. Steinberg, J.T. Ruzinski, E. Caldwell, W.B. Wong, et al., Serial changes in surfactant-associated proteins in lung and serum before and after onset of ARDS, Am. J. Respir. Crit. Care Med. 160 (1999) 1843–1850.
[27] K.R. Melton, L.L. Nesslein, M. Ikegami, J.W. Tichelaar, J.C. Clark, J.A. Whitsett, et al., SP-B deficiency causes respiratory failure in adult mice, Am. J. Physiol. Lung Cell. Mol. Physiol. 285 (2003) L543L9.
[28] M. Echaide, C. Autilio, R. Arroyo, J. Pérez-Gil, Restoring pulmonary surfactant membranes and films at the respiratory surface, Biochim. Biophys. Acta Biomembr. 1859 (2017) 1725–1739.
[29] H. Zhang, Q. Fan, Y.E. Wang, C.R. Neal, Y.Y. Zuo, Comparative study of clinical pulmonary surfactants using atomic force microscopy, Biochim. Biophys. Acta Biomembr. 1808 (2011) 1832–1842.
[30] L. Yang, J. Johansson, R. Ridsdale, H. Willander, M. Fitzen, H.T. Akinbi, et al., Surfactant protein B propeptide contains a saposin-like protein domain with antimicrobial activity at low pH, J. Immunol. 184 (2010) 975–983.
[31] B. Olmeda, B. García-Álvarez, J. Pérez-Gil, Structure–function correlations of pulmonary surfactant protein SP-B and the saposin-like family of proteins, Eur. Biophys. J. 42 (2013) 209–222.
[32] S. Hawgood, M. Derrick, F. Poulain, Structure and properties of surfactant protein B, Biochim. Biophys. Acta Mol. Basis Dis. 1408 (1998) 150–160.
[33] D.C. Beck, M. Ikegami, C.-L. Na, S. Zaltash, J. Johansson, J. A. Whitsett, et al., The role of homodimers in surfactant protein B function *in vivo*, J. Biol. Chem. 275 (2000) 3365–3370.
[34] J. Johansson, H. Jörnvall, T. Curstedt, Human surfactant polypeptide SP-B disulfide bridges, C-terminal end, and peptide analysis of the airway form, FEBS Lett. 301 (1992) 165–167.
[35] B. Olmeda, B. García-Álvarez, M.J. Gómez, M. Martínez-Calle, A. Cruz, J. Pérez-Gil, A model for the structure and mechanism of action of pulmonary surfactant protein B, FASEB J. 29 (2015) 4236–4247.
[36] V.E. Ahn, K.F. Faull, J.P. Whitelegge, A.L. Fluharty, G.G. Privé, Crystal structure of saposin B reveals a dimeric shell for lipid binding, Proc. Natl. Acad. Sci. 100 (2003) 38–43.
[37] E.J. Cabré, M. Martínez-Calle, M. Prieto, A. Fedorov, B. Olmeda, L.M.S. Loura, et al., Homo- and hetero-oligomerization of hydrophobic pulmonary surfactant proteins SP-B and SP-C in surfactant phospholipid membranes, J. Biol. Chem. 293 (2018) 9399–9411.
[38] S. Taneva, K.M.W. Keough, Cholesterol modifies the properties of surface films of dipalmitoylphosphatidylcholine plus pulmonary surfactant-associated protein B or C spread or adsorbed at the air–water interface, Biochemistry. 36 (1997) 912–922.
[39] L. Gómez-Gil, D. Schürch, E. Goormaghtigh, J. Pérez-Gil, Pulmonary surfactant protein SP-C counteracts the deleterious effects of cholesterol on the activity of surfactant films under physiologically relevant compression-expansion dynamics, Biophys. J. 97 (2009) 2736–2745.
[40] M. Manna, T. Nieminen, I. Vattulainen, Understanding the role of lipids in signaling through atomistic and multiscale simulations of cell membranes, Annu. Rev. Biophys. 48 (2019) 421–439.
[41] G. Enkavi, M. Javanainen, W. Kulig, T. Róg, I. Vattulainen, Multiscale simulations of biological membranes: the challenge to understand biological phenomena in a living substance, Chem. Rev. 119 (2019) 5607–5774.
[42] S. Baoukina, D.P. Tieleman, Computer simulations of lung surfactant, Biochim. Biophys. Acta Biomembr. 1858 (2016) 2431–2440.

[43] S. Baoukina, D.P. Tieleman, Lung surfactant protein SP-B promotes formation of bilayer reservoirs from monolayer and lipid transfer between the interface and subphase, Biophys. J. 100 (2011) 1678–1687.
[44] M.H. Khatami, I. Saika-Voivod, V. Booth, All-atom molecular dynamics simulations of lung surfactant protein B: structural features of SP-B promote lipid reorganization, Biochim. Biophys. Acta Biomembr. 1858 (2016) 3082–3092.
[45] N.A. Robichaud, M.H. Khatami, I. Saika-Voivod, V. Booth, All-atom molecular dynamics simulations of dimeric lung surfactant protein B in lipid multilayers, Int. J. Mol. Sci. 20 (2019) 3863.
[46] D.H. De Jong, G. Singh, W.F.D. Bennett, C. Arnarez, T.A. Wassenaar, L.V. Schäfer, et al., Improved parameters for the Martini coarse-grained protein force field, J. Chem. Theory Comput. 9 (2013) 687–697.
[47] J. Michalowsky, L.V. Schäfer, C. Holm, J. Smiatek, A refined polarizable water model for the coarse-grained MARTINI force field with long-range electrostatic interactions, J. Chem. Phys. 146 (2017), 054501.
[48] S.J. Marrink, H.J. Risselada, S. Yefimov, D.P. Tieleman, A.H. De Vries, The Martini force field: coarse grained model for biomolecular simulations, J. Phys. Chem. B 111 (2007) 7812–7824.
[49] L. Monticelli, S.K. Kandasamy, X. Periole, R.G. Larson, D.P. Tieleman, S.J. Marrink, The Martini coarse-grained force field: extension to proteins, J. Chem. Theory Comput. 4 (2008) 819–834.
[50] S. Baoukina, D.P. Tieleman, Direct simulation of protein-mediated vesicle fusion: lung surfactant protein B, Biophys. J. 99 (2010) 2134–2142.
[51] M.A. Ryan, X. Qi, A.G. Serrano, M. Ikegami, J. Pérez-Gil, J. Johansson, et al., Mapping and analysis of the lytic and fusogenic domains of surfactant protein B, Biochemistry. 44 (2005) 861–872.
[52] A.G. Serrano, M. Ryan, T.E. Weaver, J. Pérez-Gil, Critical structure–function determinants within the N-terminal region of pulmonary surfactant protein SP-B, Biophys. J. 90 (2006) 238–249.
[53] D. Manzanares, K. Rodriguez-Capote, S. Liu, T. Haines, Y. Ramos, L. Zhao, et al., Modification of tryptophan and methionine residues is implicated in the oxidative inactivation of surfactant protein B, Biochemistry. 46 (2007) 5604–5615.
[54] R.V. Diemel, M.M.E. Snel, L.M.G. van Golde, G. Putz, H.P. Haagsman, J.J. Batenburg, Effects of cholesterol on surface activity and surface topography of spread surfactant films, Biochemistry. 41 (2002) 15007–15016.
[55] L. Gunasekara, S. Schürch, W.M. Schoel, K. Nag, Z. Leonenko, M. Haufs, et al., Pulmonary surfactant function is abolished by an elevated proportion of cholesterol, Biochim. Biophys. Acta Mol. Cell Biol. Lipids 1737 (2005) 27–35.
[56] E. Keating, L. Rahman, J. Francis, A. Petersen, F. Possmayer, R. Veldhuizen, et al., Effect of cholesterol on the biophysical and physiological properties of a clinical pulmonary surfactant, Biophys. J. 93 (2007) 1391–1401.
[57] L. Gómez-Gil, J. Pérez-Gil, E. Goormaghtigh, Cholesterol modulates the exposure and orientation of pulmonary surfactant protein SP-C in model surfactant membranes, Biochim. Biophys. Acta Biomembr. 1788 (2009) 1907–1915.
[58] N. Roldan, T.K. Nyholm, J.P. Slotte, J. Pérez-Gil, B. García-Álvarez, Effect of lung surfactant protein SP-C and SP-C-promoted membrane fragmentation on cholesterol dynamics, Biophys. J. 111 (2016) 1703–1713.
[59] N. Roldan, J. Pérez-Gil, M.R. Morrow, B. García-Álvarez, Divide & conquer: surfactant protein SP-C and cholesterol modulate phase segregation in lung surfactant, Biophys. J. 113 (2017) 847–859.
[60] J. Ruwisch, K. Sehlmeyer, N. Roldan, B. Garcia-Alvarez, J. Perez-Gil, T.E. Weaver, et al., Air space distension precedes spontaneous fibrotic remodeling and impaired cholesterol metabolism in the absence of surfactant protein C, Am. J. Respir. Cell Mol. Biol. (2020) https://doi.org/10.1165/rcmb.2019-0358OC.
[61] F. Baumgart, O.L. Ospina, I. Mingarro, I. Rodríguez-Crespo, J. Pérez-Gil, Palmitoylation of pulmonary surfactant protein SP-C is critical for its functional cooperation with SP-B to sustain compression/expansion dynamics in cholesterol-containing surfactant films, Biophys. J. 99 (2010) 3234–3243.
[62] E. Parra, A. Alcaraz, A. Cruz, V.M. Aguilella, J. Pérez-Gil, Hydrophobic pulmonary surfactant proteins SP-B and SP-C induce pore formation in planar lipid membranes: evidence for proteolipid pores, Biophys. J. 104 (2013) 146–155.
[63] E. Parra, L.H. Moleiro, I. López-Montero, A. Cruz, F. Monroy, J. Pérez-Gil, A combined action of pulmonary surfactant proteins SP-B and SP-C modulates permeability and dynamics of phospholipid membranes, Biochem. J. 438 (2011) 555–564.
[64] M. Chavarha, R.W. Loney, S.B. Rananavare, S.B. Hall, Hydrophobic surfactant proteins strongly induce negative curvature, Biophys. J. 109 (2015) 95–105.
[65] M. Chavarha, R.W. Loney, S.B. Rananavare, S.B. Hall, An anionic phospholipid enables the hydrophobic surfactant proteins to alter spontaneous curvature, Biophys. J. 104 (2013) 594–603.
[66] I. Andre, P. Bradley, C. Wang, D. Baker, Prediction of the structure of symmetrical protein assemblies, Proc. Natl. Acad. Sci. 104 (2007) 17656–17661.
[67] C.A. Rohl, C.E.M. Strauss, K.M.S. Misura, D. Baker, Protein structure prediction using Rosetta, Methods Enzymol. 383 (2004) 66–93.
[68] M.D. Tyka, D.A. Keedy, I. André, F. DiMaio, Y. Song, D.C. Richardson, et al., Alternate states of proteins revealed by detailed energy landscape mapping, J. Mol. Biol. 405 (2011) 607–618.
[69] S.C. Li, Y.K. Ng, Calibur: a tool for clustering large numbers of protein decoys, BMC Bioinf. 11 (2010) 25.
[70] W. Humphrey, A. Dalke, K. Schulten, VMD—visual molecular dynamics, J. Mol. Graph. 14 (1996) 33–38.
[71] M.J. O'Meara, A. Leaver-Fay, M.D. Tyka, A. Stein, K. Houlihan, F. DiMaio, et al., Combined covalent-electrostatic model of hydrogen bonding improves structure prediction with Rosetta, J. Chem. Theory Comput. 11 (2015) 609–622.
[72] D.H. De Jong, S. Baoukina, H.I. Ingólfsson, S.J. Marrink, Martini straight: boosting performance using a shorter cutoff and GPUs, Comput. Phys. Commun. 199 (2016) 1–7.
[73] X. Periole, M. Cavalli, S.J. Marrink, M.A. Ceruso, Combining an elastic network with a coarse-grained molecular force field: structure, dynamics, and intermolecular recognition, J. Chem. Theory Comput. 5 (2009) 2531–2543.
[74] Abraham MJ, Murtola T, Schulz R, Páll S, Smith JC, Hess B, et al. Gromacs: high performance molecular simulations through multi-level parallelism from laptops to supercomputers. SoftwareX. 2015;1–2:19–25.
[75] I.G. Tironi, R. Sperb, P.E. Smith, Gunsteren WFv, A generalized reaction field method for molecular dynamics simulations, J. Chem. Phys. 102 (1995) 5451–5459.

[76] H. Grubmüller, H. Heller, A. Windemuth, K. Schulten, Generalized Verlet algorithm for efficient molecular dynamics simulations with long-range interactions, Mol. Simul. 6 (1991) 121–142.
[77] G. Bussi, D. Donadio, M. Parrinello, Canonical sampling through velocity rescaling, J. Chem. Phys. 126 (2007), 014101.
[78] M. Parrinello, A. Rahman, Polymorphic transitions in single crystals: a new molecular dynamics method, J. Appl. Phys. 52 (1981) 7182–7190.
[79] U. Essmann, L. Perera, M.L. Berkowitz, T. Darden, H. Lee, L. G. Pedersen, A smooth particle mesh Ewald method, J. Chem. Phys. 103 (1995) 8577–8593.
[80] S.O. Yesylevskyy, L.V. Schäfer, D. Sengupta, S.J. Marrink, Polarizable water model for the coarse-grained MARTINI force field, PLoS Comput. Biol. 6 (2010).
[81] B. Hess, H. Bekker, H.J.C. Berendsen, J.G.E.M. Fraaije, LINCS: a linear constraint solver for molecular simulations, J. Comput. Chem. 18 (1997) 1463–1472.
[82] T.A. Wassenaar, H.I. Ingólfsson, R.A. Böckmann, D.P. Tieleman, S.J. Marrink, Computational lipidomics with insane: a versatile tool for generating custom membranes for molecular simulations, J. Chem. Theory Comput. 11 (2015) 2144–2155.